

Engineering SYK interactions in disordered graphene flakes under realistic experimental conditions

Marta Brzezińska,^{1,*} Yifei Guan,^{1,*} Oleg V. Yazyev,¹ Subir Sachdev,² and Alexander Kruchkov^{1,2,3}

¹*Institute of Physics, École Polytechnique Fédérale de Lausanne, Lausanne, CH 1015, Switzerland*

²*Department of Physics, Harvard University, Cambridge, Massachusetts 02138, USA*

³*Branco Weiss Society in Science, ETH Zurich, Zurich, CH 8092, Switzerland*

We model SYK (Sachdev-Ye-Kitaev) interactions in disordered graphene flakes up to 300 000 atoms (~ 100 nm in diameter) subjected to an out-of-plane magnetic field \mathbf{B} of 5-20 Tesla within the tight-binding formalism. We investigate two sources of disorder: (i) irregularities at the system boundaries, and (ii) bulk vacancies,—for a combination of which we find conditions which could be favorable for the formation of the phase with SYK features under realistic experimental conditions above the liquid helium temperature.

There has been significant recent interest in the condensed matter community of a holographic gravitational description of correlated electron systems [1, 2]. A model in this direction is the Sachdev-Ye-Kitaev (SYK) model [3, 4], which describes from the condensed matter perspective a set of N electrons in a dispersionless quantum state (a flat band), interacting strongly yet randomly all-to-all,

$$\mathcal{H}_{\text{SYK}} = \sum_{ijkl}^N J_{ijkl} c_i^\dagger c_j^\dagger c_k c_l. \quad (1)$$

Here c_i^\dagger (c_i) are fermionic creation (annihilation) operators, and J_{ijkl} are random couplings in all indices (the model works beyond the Gaussian randomness [5]). Despite its attractive mathematical properties such as exact solvability in the large N limit with nearly conformal properties [6, 7], mapping on the Jackiw-Teitelboim gravity [8], and importance for condensed matter physics (including strange metallicity [9–11] and superconductivity on the basis of SYK model [12–14]), a direct experimental realization is currently missing.

A theoretical proposal for a potential experimental platform for the electronic SYK model, given in Ref. [15], is a graphene dot with irregular boundaries placed in an external magnetic field. Ref. [15] studied ~ 2000 atoms (5 nm in radius) in a field of ~ 3200 T. However, the magnetic fields employed in Ref. [15] exceed capabilities within the laboratory realm. Modern condensed matter facilities operate with quantum transport at magnetic fields up to 16-20 T, and the highest accessible magnetic fields in DC operation are of 45 T [16]. At the same time, graphene preparation and chemical etching procedures pose limits on the controllable size and shape of a flake, allowing flexible operational capabilities with the flakes size of hundred nanometers and above, but not for a few nanometers size. In this regard, a great challenge is to overcome these obstacles to engineer a realistic graphene flake, which could host relevant interactions in the experimentally accessible magnetic fields of 5-20 T.

In this paper we report large-scale calculations on large graphene flakes involving up to 300 000 carbon atoms

(corresponding to flake size ≈ 100 nm) placed under realistic experimental conditions. We find that upon choosing a well-disordered flake, we can reach favorable experimental conditions with SYK strength $J \sim 45$ meV (we use standard normalization $J^2 = 2N^3 \langle |J_{ijkl}|^2 \rangle$), and a mesoscopic number of SYK fermions N , typically around 40 in our calculations in the magnetic fields of 10-20 T. We further model: (i) the role of chemical etching [17], or local anodic oxidation with an atomic force microscopy (AFM) tip [18–20], by varying the shape of the flake and the size of edge disorder. (ii) the role of bulk vacancies created, for example, by focused ion beam (FIB) patterning [21] or hydrogen plasma treatment [22]. Our results speak in favor of formation of SYK-like interactions in the realistic range of parameters. In particular, we point out how the relative effect of melonic diagrams can be enforced by controlling the atomic vacancies concentration in the bulk. By comparing the relevant energy scales [23], namely t^2/J and J/N , we come to the conclusion that the engineered system has a set of parameters where it could realize the SYK phase in the vicinity of the liquid helium operational temperatures, accessible magnetic fields, and suitable graphene flake scales.

Setup. To construct the SYK model, one needs to employ the dispersionless quantum states (flat bands), in particular electronic states with nontrivial Bloch topology. Such flat band states have been classified in Ref. [24]. The simplest of this construction are the Landau levels, which are characterized by Chern number $|C|=1$. In principle, one can use numerous 2D materials for this purpose, however we here limit ourselves to the case of graphene [15] for two reasons: (i) graphene monolayer is an intuitively understood system from both analytical and numerical viewpoint; (ii) there are existing experimental platforms satisfying criteria for this direction [25].

Before proceeding to disordered graphene flakes, let us recall the physics of pristine (homogeneous and boundless) graphene in low-energy approximation. Upon application of out-of-plane magnetic field B , the electronic spectrum of pristine graphene is given by [26]

$$E_n = \pm v_F \sqrt{2\hbar e B |n|}, \quad (2)$$

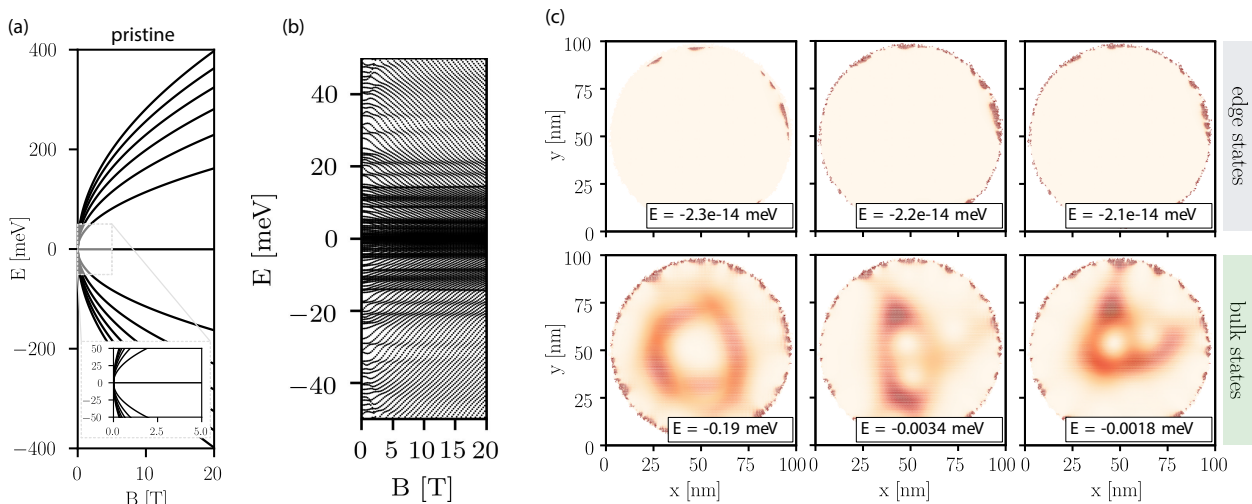


FIG. 1. **Bulk and edge states in disordered graphene flake of 100 nm in strong magnetic fields.** (a) Energy spectrum as a function of magnetic field, expected in pristine graphene; inset shows the same spectrum in energy range $[-50 \text{ meV}; +50 \text{ meV}]$ to compare with panel (b); (b) De-facto energy spectrum, observed in a strongly disordered graphene flake of size 100 nm; higher Landau levels ($|n| > 0$) are not recognized in the energy range $[-50, +50 \text{ meV}]$; (c) probability densities $|\psi|^2$ of exemplary bulk and edge states. Randomly localized bulk states shown in bottom of (c) are the building blocks for constructing the SYK-like interactions (Fig. 2).

where e is electronic charge and $v_F \approx 10^6 \text{ m/s}$ is the Fermi velocity. The lowest Landau level (LLL) is characterized by zero modes in the bulk ($n=0$). In the presence of chiral symmetry, the Aharonov-Casher argument [27] sets the number of electronic states in LLL as

$$N_0 = \frac{BA}{\Phi_0}, \quad (3)$$

where A is the flake area, and $\Phi_0 = h/e = 4.136 \cdot 10^{-15} \text{ Wb}$ is the magnetic flux quantum. N_0 in Eq. (3) sets the order of magnitude for the number N of SYK states in the Hamiltonian in Eq. (1), however we see that N within bandwidth $t = 2 \text{ meV}$ around the Fermi level N is fluctuating around N_0 due to strong disorder effects in considered graphene flakes (see Fig. 2). Still there is a certain qualitative similarity with the ideal LLL case, even that the flake is strongly disordered.

The typical electronic spectrum of a strongly disordered graphene flake is illustrated in Fig. 1. The flake has a disorder-free inner region of radius R_1 , followed by disordered edge up to radius R_2 (46 nm and 50 nm in Figs. 1, 2). Tight-binding (TB) calculations are performed with the conventional graphene model in magnetic fields [28], taking into account nearest-neighbors hoppings with Peierls substitution [29]. Figure 1 shows the results obtained from diagonalization of the TB model describing the 100 nm flake consisting of around 270 000 of atoms. The first observation is that the electronic spectrum of a realistic disordered flake in the relevant energy range deviates significantly from its pristine counterpart, given by Eq. (2): in all the realistic magnetic fields 0 to 20 T, we no longer observe the square-root behavior of eigenener-

gies as expected for pristine graphene; instead, the spectrum acquires a quantum-dot-like distribution [30].

We distinguish the bulk states from the edge states through the analysis of their localization properties. For this, we integrate $|\Psi|^2$ within radius $R_1 + \delta$ ($\delta \rightarrow 0$) [31]. Due to the presence of irregularities on the boundaries, all the states are showing certain localization at the edge; however bulk states have significant weight in bulk. If at least 50% of weight is localized in bulk, we label this state as a bulk state (In the Supplementary Material, we show that a different criterion, based on analysis of inversed participation ratio (IPR), leads to qualitatively similar results). While, as expected, the edge states are strongly localized at the irregular boundaries, the bulk states sway over all the flake diameter, being spread on the length scale of $\sim 100 \text{ nm}$. With such large length scale over which the bulk states are spread, the notion of distance is lost, and these states are interacting randomly all-to-all, in the SYK spirit.

Calculation of the SYK terms. With the bulk states randomly localized, and the kinetic energy quenched to $t < 2 \text{ meV}$, we construct the SYK-like states by introducing the Coulomb interaction in the basis of randomized bulk states [15, 32]. We compute Sachdev-Ye-Kitaev interaction terms through

$$J_{ijkl} = \frac{1}{2} \sum_{\mathbf{r}_1} \sum_{\mathbf{r}_2} \Psi_i^*(\mathbf{r}_1) \Psi_j^*(\mathbf{r}_2) U(\mathbf{r}_1 - \mathbf{r}_2) \Psi_k(\mathbf{r}_1) \Psi_l(\mathbf{r}_2) \quad (4)$$

where $U(\mathbf{r})$ is the screened Coulomb potential. Our results stand for different forms of the screened Coulomb potentials. To be specific, we adopt the values of renor-

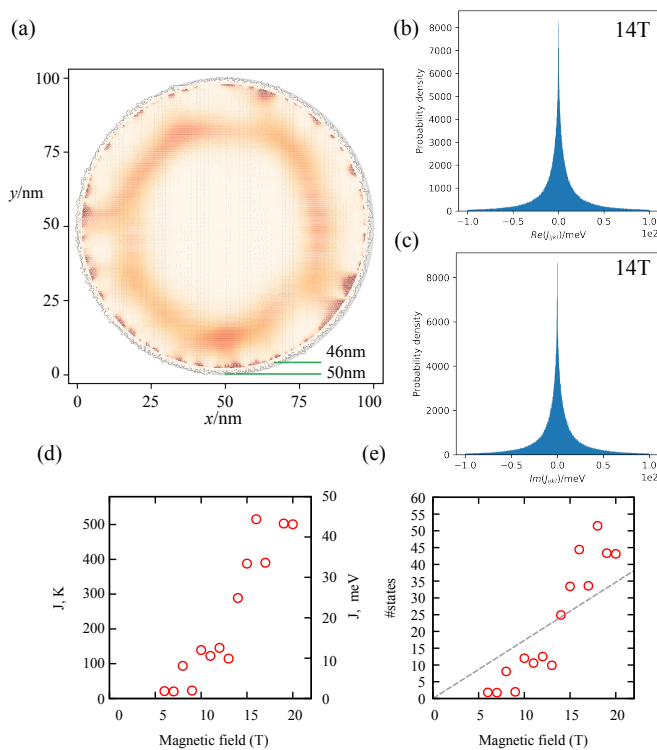


FIG. 2. **SYK-like interactions in the graphene flake of size 100 nm** (268'510 Carbon atoms) under realistic magnetic fields 5-20 T. (a) The geometry of the flake used for numerical modeling, together with the visualization of a typical bulk state near the Fermi level. (b-c) Distribution of real and imaginary parts J_{ijkl} terms computed from Eq. (4) with $\text{Re}\langle J_{ijkl} \rangle \approx 0$ and $\text{Im}\langle J_{ijkl} \rangle \approx 0$. (d) The value of SYK interaction J , determined by the second moments in Eq. (5). For calculation, we take bulk states distributed between $[-1 \text{ meV}, +1 \text{ meV}]$ around the Fermi level. Panel (e) shows number of bulk states in the range $[-1 \text{ meV}, +1 \text{ meV}]$ involved into J_{ijkl} calculation; gray dashed line depicts ideal LLL case Eq.(3).

malized interaction potentials for graphene as it was reported in Refs. [33]. In particular, we adopt $U_{\text{NN}} = 5.5 \text{ eV}$, $U_{\text{NNN}} = 4.1 \text{ eV}$, $U_{\text{NNNN}} = 3.6 \text{ eV}$, where (N)NN stands for (next)-nearest neighbor interactions. In calculation of J_{ijkl} terms (4), we take only bulk states within the energy range $[-1 \text{ meV}, +1 \text{ meV}]$ around the neutrality. This qualitatively corresponds to focusing on the states associated with what used to be LLL (see dashed line in Fig.2e), similar to Ref. [15]. For medium size flakes, we check that changing the bulk states range $[-1 \text{ meV}, +1 \text{ meV}]$ to $[-5 \text{ meV}, +5 \text{ meV}]$ does not change significantly the results for J_{ijkl} calculations, since most of the bulk states are situated near the zero energy, and higher excited bulk states contribute marginally to SYK interactions J_{ijkl} . Hence, in what follows we proceed with bulk states within $[-1 \text{ meV}, +1 \text{ meV}]$.

The key results for the large flake are summarized in Fig. 2. The statistical distribution of the complex-valued

J_{ijkl} terms is illustrated in Fig. 2(bc). The mean is zero, ($\text{Re}\langle J_{ijkl} \rangle \approx 0$, $\text{Im}\langle J_{ijkl} \rangle \approx 0$), which indicates that real and imaginary parts of J_{ijkl} are independent. The overall distribution of the absolute values of J_{ijkl} (in Fig. 2(c)) is quasirandom, but non-Gaussian as in conventional SYK models [6, 7]; however, this is not the problem for constructing SYK-like models [5]. We introduce the real-valued strength of SYK interactions J as with normalization from counting melonic diagrams [7]

$$J = \sqrt{2}N^{3/2} \langle J_{ijkl} J_{ijkl}^* \rangle^{1/2}. \quad (5)$$

We operate this quantity in meV and Kelvin for practical convenience. The results for the large flake are encouraging, with extracted J of around 35 meV at 15 T (see Fig. 2(d)). The number of SYK fermions peaks to 50-60 and we typically take around 40 of them for our calculations.

Dependence on edge disorder scale. We next address the question of how the edge disorder $\chi = (R_2 - R_1)/R_2$ influences the SYK interaction strength J . This question is vital for the experiments, where only a limited number of methods is available for shaping the flake of the size of 100-200 nm (chemical etching, FIB, hydrogen plasma treatment). To optimize the numerical costs, we now turn to the medium size flakes of diameter 60 nm ($\sim 100\,000$ atoms); these results are rescalable towards large graphene flake of size 300 000 atoms and more as in prototypes [25]. We observe that the strength of the SYK interaction J can be tuned by increasing the edge disorder χ (see Fig. 3). To quantify this effect we perform disorder averaging over dozens of flakes (Fig 3 uses up to 20 flake realizations). Typically J scatters from 5-10 meV to nearly 60 meV upon increasing χ from 0 to 20%, but some samples may exhibit even larger values of J above 80 meV (outside of plot range in Fig. 3) in the intermediate regime. Comparing with Fig. 2, we come to the conclusion that the energy scale $J \sim 20\text{-}40 \text{ meV}$ is

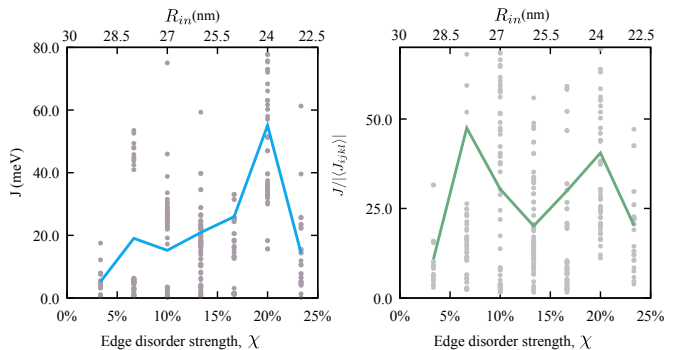


FIG. 3. **Enhancing SYK interactions through edge disorder χ .** (a) SYK coupling strength J , (b) dimensionless ratio $J/|\langle J_{ijkl} \rangle|$ as a function of edge disorder scale χ for the medium size flake at $B = 20 \text{ T}$ (approx. 100 000 atoms, 60 nm in diameter). Solid lines correspond to the average over up to 20 disorder realizations (marked with grey points, some outside of plot range).

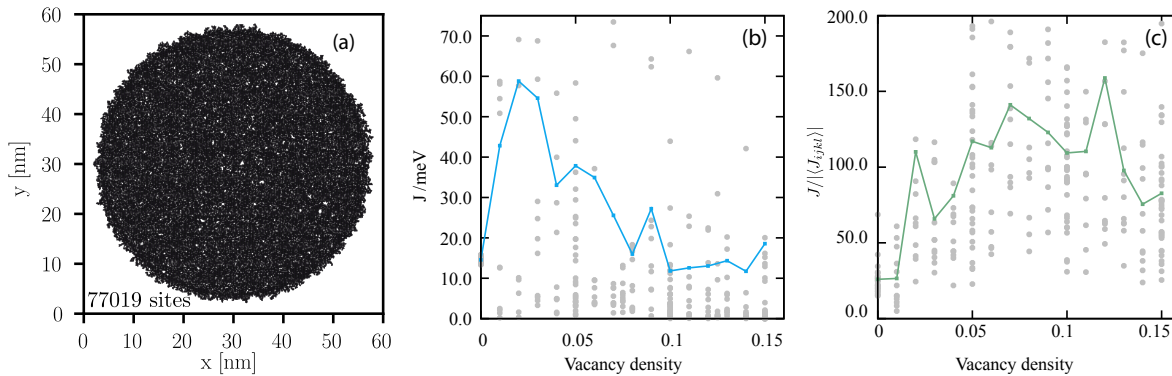


FIG. 4. **Tuning SYK strength J with vacancy patterning.** (a) illustration of the graphene flake with bulk atomic vacancies (approx. 77 000 atoms); (b) SYK strength J and (c) $J/|\langle J_{ijkl} \rangle|$ ratio as a function of the vacancies concentration in the range from 0 % to 15 % of vacancies. Solid blue lines correspond to arithmetic average over 20 disorder realizations in the medium size flake with $R_1 = 26$ nm and $R_2 = 30$ nm at $B = 20$ T (some data points (grey) are outside of the plot range, see SM for details). At 2 % of vacancy concentration, we observe a clear maximum of SYK strength $J \sim 60$ meV. Above 15 %, the long-range order is destroyed for some disorder realizations and around 30 %, all the systems are close to the percolation threshold for hexagonal lattice $p \approx 0.7$ [34, 35].

the most robust for the experiments. Moreover, the ratio of $J/|\langle J_{ijkl} \rangle|$ in Fig. 3(b), which qualitatively points to the dominance of the melonic diagrams in the large- N limit, increases under edge disorder.

Dependence on bulk vacancies and their concentration. Another mechanism of control is behavior vacancies implanting as in Fig 4(a), performed e.g. via FIB tools. In this case, the sample patterning can provide additional tuning knob to improve the properties towards SYK-like behavior. We here perform the calculations for the medium size flakes of 60 nm in $B = 20$ T. The results are shown in Fig. 4. We start with the flake which has only moderate (non-optimized) edge disorder, reflected in $J \approx 15$ meV, and gradually increase the number atomic vacancies. Fig 4(b) gives the dependence of the SYK interaction J versus vacancy concentration in the bulk. The first effect of vacancies patterning is a peak around 2% concentration with $J \approx 60$ meV and then the decrease of SYK coupling J back to 10-20 meV at 15 % concentration. The number of bulk states slowly grows with a vacancy concentration (see SM); we check that the bulk states are not exponentially localized on the atomic vacancies. In Fig. 4(c), the ratio $J/|\langle J_{ijkl} \rangle|$ is improved by adding a moderate amount of vacancies (at 0 % this ratio is $J/|\langle J_{ijkl} \rangle| \approx 25$, at 2 % it is $J/|\langle J_{ijkl} \rangle| \approx 110$), hence promoting the role of melonic diagrams [7]. Therefore, we come to conclusion that even a modest vacancy concentration of 2% improves the properties of the SYK flake. For the flakes of size 100 nm, we recommend removing ~ 6000 Carbon atoms.

Discussion of the temperature scales. Finally, we perform the analysis of the relevant energy scales. The key energy scale is $J \approx 35$ meV (taken at experimentally relevant $B = 16$ T from Fig. 2). The SYK model is

well-defined in the region $T \ll J$. Furthermore, there are lower bounds on the temperature coming from (i) finite bandwidth of the flat band, and (ii) mesoscopic effects in the SYK Hamiltonians. Both these temperature scales appear in quantum transport treatment of the SYK island [23]. The first temperature bound is set by the bandwidth t . However, the question of the bandwidth for strongly-disorder flakes is not well defined; from Fig. 1b we estimate the upper bounds as ± 15 meV, from which we estimate $t \approx 7.5$ meV; similar upper bounds are imposed by experiment [36]. This gives $T_1 = t^2/J \approx 19$ K. Around this value, the SYK dynamics crossover to conventional Fermi liquid behavior in a universal manner. The second temperature scale is set by the mesoscopic number of SYK states. In our case of a large flake ($N \approx 35$), $T_2 = J/N \approx 10$ K. Below T_2 , mesoscopic fluctuations are described by the universal Schwarzian theory of the SYK model (with possible perturbations from t) [23]. Therefore, we come to conclusion that in the magnetic fields of 16 T, flake sizes of order 100 nm, the SYK dynamics is most favorable in the regime $20 \text{ K} \lesssim T_{\text{SYK}} \ll 300 \text{ K}$. We hence expect the signatures of SYK model [7] in this temperature range, and probe the relevant quantum transport, namely conductance and thermopower, in this regime [23]. This allows to operate the 100 nm graphene flakes of Figs. 1, 2 above the point of the liquid helium temperature ($T_{\text{He}} = 4.2$ K), a relevant experimental benchmark.

Conclusions. In conclusion, by performing large-scale calculation on up to 300 000 atomic sites, we have demonstrated that the SYK interactions can be controllably engineered and enhanced in the disordered graphene flake in realistic magnetic fields 5-20 T, when the flake enters the

quantum dot regime. The obtained results speak in favor of underlying SYK dynamics in the disordered graphene flakes, establishing realistic experimental conditions in terms of length scales, temperatures, and magnetic fields. Further theoretical modelling of transport across such disordered graphene flakes is required to interpret the graphene prototypes behavior in experiments [25].

Acknowledgements. We thank Philip Kim, Bertrand Halperin, Laurel Anderson for useful discussion. This work was supported by the Branco Weiss Society in Science, ETH Zurich, through the research grant on flat bands, strong interactions and the SYK physics. Computations have been performed at the Swiss National Supercomputing Centre (CSCS) and the facilities of Scientific IT and Application Support Center of EPFL. S.S. were supported by the National Science Foundation under Grant No. DMR-2002850 and by the Simons Collaboration on Ultra-Quantum Matter, a grant from the Simons Foundation (651440). Y.G. and O.V.Y. acknowledge support from the Swiss National Science Foundation (grant No. 204254).

* These two authors contributed equally.

- [1] S. A. Hartnoll, A. Lucas, and S. Sachdev, *Holographic quantum matter* (MIT press, 2018).
- [2] S. A. Hartnoll, Lectures on holographic methods for condensed matter physics, *Classical and Quantum Gravity* **26**, 224002 (2009).
- [3] S. Sachdev and J. Ye, Gapless spin-fluid ground state in a random quantum Heisenberg magnet, *Physical Review Letters* **70**, 3339 (1993).
- [4] A. Kitaev, A simple model of quantum holography, Talks at KITP (2015).
- [5] T. Krajewski, M. Laudonio, R. Pescalie, and A. Tanasa, Non-Gaussian disorder average in the Sachdev-Ye-Kitaev model, *Physical Review D* **99**, 126014 (2019).
- [6] J. Maldacena and D. Stanford, Remarks on the Sachdev-Ye-Kitaev model, *Physical Review D* **94**, 106002 (2016).
- [7] Y. Gu, A. Kitaev, S. Sachdev, and G. Tarnopolsky, Notes on the complex Sachdev-Ye-Kitaev model, *Journal of High Energy Physics* **2020**, 1 (2020).
- [8] A. Kitaev and S. J. Suh, The soft mode in the Sachdev-Ye-Kitaev model and its gravity dual, *Journal of High Energy Physics* **2018**, 183 (2018).
- [9] A. Haldar and V. B. Shenoy, Strange half-metals and mott insulators in Sachdev-Ye-Kitaev models, *Physical Review B* **98**, 165135 (2018).
- [10] P. Cha, N. Wentzell, O. Parcollet, A. Georges, and E.-A. Kim, Linear resistivity and Sachdev-Ye-Kitaev (SYK) spin liquid behavior in a quantum critical metal with spin-1/2 fermions, *Proceedings of the National Academy of Sciences* **117**, 18341 (2020).
- [11] D. Chowdhury, A. Georges, O. Parcollet, and S. Sachdev, Sachdev-Ye-Kitaev Models and Beyond: A Window into Non-Fermi Liquids, (2021), arXiv:2109.05037.
- [12] H. Wang, A. L. Chudnovskiy, A. Gorsky, and A. Kamenev, Sachdev-Ye-Kitaev superconductivity: Quantum Kuramoto and generalized Richardson models, *Physical Review Research* **2**, 033025 (2020).
- [13] L. Classen and A. Chubukov, Superconductivity of incoherent electrons in the Yukawa Sachdev-Ye-Kitaev model, *Physical Review B* **104**, 125120 (2021).
- [14] G.-A. Inkof, K. Schalm, and J. Schmalian, Quantum critical Eliashberg theory, the Sachdev-Ye-Kitaev superconductor and their holographic duals, *NPG Quantum Materials* **7**, 1 (2022).
- [15] A. Chen, R. Ilan, F. De Juan, D. Pikulin, and M. Franz, Quantum holography in a graphene flake with an irregular boundary, *Physical Review Letters* **121**, 036403 (2018).
- [16] S. Hahn, K. Kim, K. Kim, X. Hu, T. Painter, I. Dixon, S. Kim, K. R. Bhattarai, S. Noguchi, J. Jaroszynski, *et al.*, 45.5-Tesla direct-current magnetic field generated with a high-temperature superconducting magnet, *Nature* **570**, 496 (2019).
- [17] L. Wang, I. Meric, P. Huang, Q. Gao, Y. Gao, H. Tran, T. Taniguchi, K. Watanabe, L. Campos, D. Muller, *et al.*, One-dimensional electrical contact to a two-dimensional material, *Science* **342**, 614 (2013).
- [18] R. Puddy, P. Scard, D. Tyndall, M. Connolly, C. Smith, G. Jones, A. Lombardo, A. Ferrari, and M. Buitelaar, Atomic force microscope nanolithography of graphene: cuts, pseudocuts, and tip current measurements, *Applied Physics Letters* **98**, 133120 (2011).
- [19] S. Masubuchi, M. Arai, and T. Machida, Atomic force microscopy based tunable local anodic oxidation of graphene, *Nano Letters* **11**, 4542 (2011).
- [20] H. Li, Z. Ying, B. Lyu, A. Deng, L. Wang, T. Taniguchi, K. Watanabe, and Z. Shi, Electrode-free anodic oxidation nanolithography of low-dimensional materials, *Nano Letters* **18**, 8011 (2018).
- [21] B. Archanjo, A. Barboza, B. Neves, L. Malard, E. Ferreira, J. Brant, E. Alves, F. Plentz, V. Carozo, B. Fragneaud, *et al.*, The use of a Ga⁺ focused ion beam to modify graphene for device applications, *Nanotechnology* **23**, 255305 (2012).
- [22] E. Despiau-Pujo, A. Davydova, G. Cunge, and D. B. Graves, Hydrogen plasmas processing of graphene surfaces, *Plasma Chemistry and Plasma Processing* **36**, 213 (2016).
- [23] A. Kruchkov, A. A. Patel, P. Kim, and S. Sachdev, Thermoelectric power of Sachdev-Ye-Kitaev islands: Probing Bekenstein-Hawking entropy in quantum matter experiments, *Physical Review B* **101**, 205148 (2020).
- [24] A. Kruchkov, Quantum geometry, flat Chern bands, and Wannier orbital quantization, *Physical Review B* **105**, L241102 (2022).
- [25] L. Anderson, A. Laitinen, A. Kruchkov, K. Watanabe, T. Taniguchi, and P. Kim, Electrical and thermoelectric transport in random-edged graphene quantum dots in the lowest Landau level, *Bulletin of the American Physical Society* (2022).
- [26] V. Gusynin and S. Sharapov, Unconventional integer quantum Hall effect in graphene, *Physical Review Letters* **95**, 146801 (2005).
- [27] Y. Aharonov and A. Casher, Ground state of a spin-1/2 charged particle in a two-dimensional magnetic field, *Physical Review A* **19**, 2461 (1979).
- [28] M. O. Goerbig, Electronic properties of graphene in a strong magnetic field, *Rev. Mod. Phys.* **83**, 1193 (2011).

- [29] For computational advance, we combine KWANT toolbox [37] with FEAST algorithms [38].
- [30] We note however that in much stronger magnetic flux $\sim h/e$, the well-defined structure from Eq. (2) reappears.
- [31] For numerical purposes, we use $\delta = 0.1(R_2 - R_1)$ in the calculations in the main text.
- [32] C. Wei and T. A. Sedrakyan, Optical lattice platform for the Sachdev-Ye-Kitaev model, *Physical Review A* **103**, 013323 (2021).
- [33] T. O. Wehling, E. Şaşıoğlu, C. Friedrich, A. I. Lichtenstein, M. I. Katsnelson, and S. Blügel, Strength of effective Coulomb interactions in graphene and graphite, *Physical Review Letters* **106**, 236805 (2011).
- [34] P. N. Suding and R. M. Ziff, Site percolation thresholds for archimedean lattices, *Physical Review E* **60**, 275 (1999).
- [35] X. Feng, Y. Deng, and H. W. Blöte, Percolation transitions in two dimensions, *Physical Review E* **78**, 031136 (2008).
- [36] Y. Zhang, Z. Jiang, J. P. Small, M. S. Purewal, Y.-W. Tan, M. Fazlollahi, J. D. Chudow, J. A. Jaszczak, H. L. Stormer, and P. Kim, Landau-level splitting in graphene in high magnetic fields, *Phys. Rev. Lett.* **96**, 136806 (2006).
- [37] C. W. Groth, M. Wimmer, A. R. Akhmerov, and X. Waintal, Kwant: a software package for quantum transport, *New Journal of Physics* **16**, 063065 (2014).
- [38] E. Polizzi, Density-matrix-based algorithm for solving eigenvalue problems, *Physical Review B* **79**, 115112 (2009).